GMR
The Original

COMPARATIVE BIOMECHANICAL ANALYSIS OF ARTHROPLASTY AND HEMIARTHROPLASTY HIP IMPLANTS USING ADVANCED COMPOSITE BIOMATERIALS

[1*]Siddharth Tiwari, [2]Nitin Kumar Jain

[1]Research Scholar, Department of Mechanical Engineering, NIT, Raipur, India, Email: siddharthsantosh7@gmail.com
[2]Professor, Department of Mechanical Engineering, NIT, Raipur, India, Email: nkjain.me@nitrr.ac.in

ABSTRACT
Hip implant failure due to stress shielding, excessive contact pressure, and poor load transfer remains a critical clinical challenge in orthopaedic biomechanics, often leading to implant loosening and revision surgeries. This study aims to systematically evaluate the biomechanical performance of hip implant systems by conducting a comparative finite element analysis of arthroplasty and hemiarthroplasty configurations, with particular emphasis on the combined effects of stem taper geometry and advanced biomaterials. A three-dimensional femoral model derived from computed tomography data was analyzed under physiological loading conditions ranging from 2200 N to 2800 N. Three implant materials—NbTiZrMo alloy, PEEK, and CFR-PEEK—were assessed in terms of equivalent elastic strain, Von Mises stress, and contact pressure. The results demonstrate that CFR-PEEK achieves a significant reduction in implant stress (approximately 18–25%) compared to NbTiZrMo alloy, while maintaining substantially lower deformation than PEEK. Furthermore, hemiarthroplasty configurations exhibit 8–12% lower stress levels and reduced contact pressures relative to arthroplasty under identical loading conditions, indicating improved load-sharing capability due to the natural acetabular interface. Unlike prior studies that primarily focused on isolated parameters, the present work introduces an integrated evaluation framework combining implant configuration, taper geometry, and material selection. The findings highlight the superior biomechanical balance of CFR-PEEK and underscore its potential to minimize stress shielding and enhance implant longevity, offering clinically relevant insights for optimizing hip replacement design and reducing long-term failure rates.

KEYWORDS: Hip arthroplasty; Femur Head; Finite Element Analysis; Arthroplasty; Hemiarthroplasty

1. INTRODUCTION

Total hip joint disorders such as osteoarthritis, avascular necrosis, and traumatic fractures are among the leading causes of disability worldwide, significantly affecting mobility and quality of life. Surgical intervention in the form of Total Hip Arthroplasty (THA) and Hemiarthroplasty (HA) has become a well-established and effective solution for restoring joint function and alleviating pain [1]. In THA, both the femoral head and acetabular components are replaced, whereas HA involves replacement of only the femoral head, making it a preferred option in specific clinical conditions such as femoral neck fractures in elderly patients [2].
One of the most restricting bones in the human body is the femur because of the weight it carries. The femur serves as a shock absorber while one moves about, be it walking or running [3]. The hip joint is a ball and socket joint with powerful muscles and ligatures surrounding it [4]. Total hip arthroplasty is one of the most important surgeries of the 20th century [5]. Total hip arthroplasty is the replacement of a damaged hip with an artificial one. Osteoporosis, rheumatoid, inflammation-osteoporosis, avascular necrosis, lupus, trochanteric bursitis, and coxa saltans are chronic painful diseases of the hips. With the total hip arthroplasty, the patient can move with the same range of motion as a healthy hip joint would provide prior to the injury [6]. There are now more modular and non-modular hip implants on the market than before and they come in a multitude of speculated designs. The reason for most these being used is due to the better mechanical modular hip implants offer [7, 8].

1.1 Influence of Geometry and Taper Design

All these are combined together so that they can mimic the functions of a natural femur. The critical complications with total hip arthroplasty are dislocation and aseptic loosening [9-11]. In order to enhance the understanding of head neck corrosion in hip joint implants [12]. In order to evaluate the corrosion level at head and neck taper junction, the authors studied the retrieval implants. There exists a variety of design and combination of materials that are different [13-15]. Co-Cr-Mo alloys and titanium alloys are a couple of the commonly used material pairings [16]. Many researchers have studied the effect of taper sizes on hip implants for many years.

The femoral neck adaptability joint only contributes towards motion at a hip joint [17]. It concluded that femoral neck modularity is one of the most important factors that will affect the post-operative range of motion that can

be achieved. The geometry of neck and taper on stability of implants was calculated in vivo damage to the head-neck junction and also studied the combination of metal with the femoral head [18]. The taper size was examined regarding taper damages in retrieved metal-on-polyethylene surgical implants [19]. The wear rate of a modular hip implant taper joint was checked with different manufacturing tolerances and forces on the implant [20].
All the studies mainly focused on the interaction between the dimensions of the femoral head, geometry of taper, and material combinations used in total hip replacement. But they will change as per changing boundary conditions and due to everyday activities engaged in by patients who have had total hip arthroplasty. However, conventional boundary conditions and effect taper length is not emphasized by any of the earlier publications when there is a change in femoral head size.

1.2 Arthroplasty vs Hemiarthroplasty: Comparative Insights

In a study, researchers used finite element analysis to determine the femur bone's corresponding contact forces and stress distribution. Solid Edge V19 is used to model the femur bone, while ANSYS 14.0 is used to analyse the stress. For movements such regular walking, standing, sprinting, and jumping, the femur bone's stress at the hip joint is analysed. When the results were compared to those of the previous studies, it was observed that the FEA results were optimized [21-23]. Finite element analysis of the femur bone, is represented by computer tomography (CT) scans [24]. A gait analysis is conducted and contrasted with earlier research. In relation to a single cycle, the typical stresses and pressures for standing and walking were examined. When it came to hip joint arthroplasty and hip joint implant research, the orthopaedic surgeon considered the data to be helpful [25]. The forces exerted on the femur neck during acetabular fractures have been studied computationally and by finite element analysis. Studying the acetabulum and femoral head's load-bearing capability becomes essential due to the femur bone's medical condition in osteoporosis of senior people [26]. In order to lower the risk of femoral neck fractures, numerous studies assess the articulation of the femur bone in certain circumstances. Finite element analyses are used to investigate it. The computed tomography (CT) images are used to generate a finite model of the femoral neck, and the acetabulum is subjected to a point force [27]. Deformation and stress levels were noted at the neck area, whereas the point loads at the femur head's tip varied. It is found that when the point load moves away from the centre, the stress increases. Additionally, it is discovered that when the point load is positioned differently, the bending moment in the medial neck shaft increases. Ultimately, it was determined that individuals with diseases such as osteoporosis are more likely to experience femur neck failure [28]. To investigate its potential uses as a femoral head implant in the event of total hip replacement, researchers have created a ceramic and metal composite made of silicon carbide nanoparticles reinforced with aluminium oxide and niobium. The composite samples were created by hot pressing powders at 1425 °C and 35 MPa of pressure. They were then subjected to mechanical testing and electron microscopy under various conditions. When compared to other laminates, it was found that the aluminium oxide niobium silicon carbide composite laminate had the highest flexural strength and interfacial shear strength. In comparison to aluminium oxide and other materials, it was determined that the aluminium oxide niobium silicon carbide composite has more advantageous properties for femur head applications [29-33]. In a study, scientists created a process for compressing and sintering zirconia-toughened alumina (ZTA) in order to use it as a femur head implant [31]. The generated implant was found to have remarkable qualities, including a smoother surface and more noticeable geometrical compliance. Using micro-computed tomography, the relationship between the microstructure created and the producing process was explained [32,33]. The burst strength measuring method was used to analyse the mechanical strength. An in vitro cell culture analysis was conducted to confirm or assess the implant femur head's biocompatibility [34,35]. The most important cause of failure in total hip arthroplasty is wear on the hip implant's bearing surface, which can result in osteolysis. The oxide-coated zirconium niobium femoral head was analysed and contrasted with the cobalt-chromium femoral head in a study that looked at zirconia toughened alumina. The cobalt-chromium femur head was used to compare the results of the wear abrasion investigation [36]. This study also tests the impact of ceramic on metal. In comparison to cobalt-chromium femur implants, zirconia toughened alumina and oxide-coated zirconium niobium femoral heads are found to have greater wear resistance [37-40].
During the literature study, it was discovered that the earlier researchers primarily concentrated on the many design factors that affect the hip implant's performance under static loading conditions, such as taper radius mismatch, stem lengths, and femoral head size [41-43]. Previous research has shown that the impact of femoral head length on taper length has not yet been studied and requires further investigation. Therefore, the current study uses ANSYS R-16.2 and the finite element (FE) approach to examine how femoral head length affects taper length. The boundary and loading conditions were established using the ASTM F2996-13 standards. Meshing type: tetrahedral, Mesh size: Not fixed, loading conditions: 2200 – 2500 N and Materials: NbTiZrMo alloy, PEEK, and CFR-PEEK.
This study aims to ensure methodological consistency and clinical relevance, the biomechanical boundary conditions adopted in this study are defined in accordance with the ASTM F2996-13 standard, which specifies loading configurations and constraints for the evaluation of femoral hip implant systems under physiologically representative conditions. The applied loading range and fixation approach are selected to replicate in vivo hip joint forces during daily activities, thereby enabling a reliable assessment of implant performance.
Although several studies have investigated the effects of femoral head size, taper mismatch, and material combinations, the influence of stem taper length and its interaction with advanced biomaterials such as CFR-PEEK under realistic loading conditions remains inadequately explored. In contrast to existing studies that predominantly examine femoral head dimensions or conventional material combinations, the present work

introduces a focused investigation on the influence of stem taper length in conjunction with advanced biomaterials, particularly carbon fiber–reinforced PEEK (CFR-PEEK). This study provides a systematic evaluation of how taper geometry interacts with material stiffness to affect stress distribution, load transfer, and implant stability. By integrating taper design parameters with a comparative assessment of CFR-PEEK against metallic and polymeric counterparts, the work establishes a novel framework for optimizing hip implant performance beyond traditional design considerations. Furthermore, a direct comparative analysis between arthroplasty and hemiarthroplasty using FEA is still limited in the existing literature.

Despite the widespread success of hip replacement procedures, long-term clinical outcomes are still compromised by biomechanical complications such as stress shielding, implant loosening, and progressive bone resorption. These issues are primarily associated with stiffness mismatch between the implant and surrounding bone, as well as suboptimal load transfer at the bone–implant interface, which can accelerate periprosthetic bone loss and ultimately lead to implant instability [44,45]. In addition, elevated contact stresses and micro-motions at modular junctions further contribute to wear, corrosion, and eventual failure of the implant system. Therefore, improving the biomechanical compatibility of implant materials and optimizing structural design parameters are critical to enhancing implant longevity and reducing the need for revision surgeries

1.3 Research Gap and Motivation

Although prior research has extensively addressed material selection, femoral head dimensions, and taper mismatch effects, a clear gap exists in the integrated evaluation of stem taper length in combination with advanced biomaterials such as CFR-PEEK. Furthermore, a systematic and quantitative comparison between arthroplasty and hemiarthroplasty configurations under standardized loading conditions is still lacking. Addressing this gap is essential for understanding the coupled influence of material properties and geometric design on implant stability, stress shielding, and long-term clinical performance.

2. Arthroplasty and Hemiarthroplasty

In a total hip replacement, the damaged joint is removed and replaced with a prosthesis—a piece made of any biocompatible material, such as metal, plastic, or ceramic. Because it replicates the joint's motion and movement in a compatible manner, the prosthesis design is crucial [40, 45]. Based on whether the transplant includes the patient's original bone or biomaterial acetabulum, there are two main categories of hip transplants. Hemiarthroplasty is the lack of the biomaterial acetabulum, whereas arthroplasty is its presence. Figure 1 illustrates the distinction between arthroplasty and hemiarthroplasty.

Hemiarthroplasty is a surgical procedure in which half of a joint is replaced with an artificial replacement to preserve the other half in its original state. Hemiarthroplasty is chosen over total arthroplasties due to advantages such shorter recuperation and surgical times and the preservation of more natural tissue. Notwithstanding all of these advantages, one of the primary drawbacks of the aforementioned procedure is that it accelerates the deterioration of the original or natural cartilage against which it articulates. Because osteoarthritis is the primary cause of joint replacement surgeries, these procedures are common in the senior population, which is defined as those over 60. Acetabular injury, a natural tissue, is the primary cause of hip hemiarthroplasty problems. There will always be this shape mismatch between the implants and the anatomy.

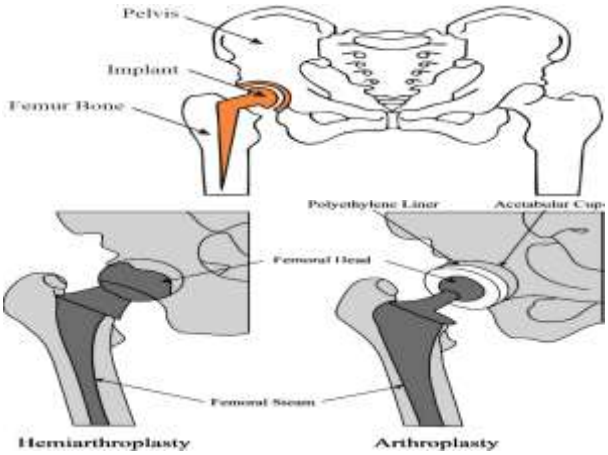

Figure 1. Human hip natural femur bone and the artificial implant (left), hemiarthroplasty and arthroplasty (right) [44]

This will cause the implant to loosen, which will result in the most frequent hemiarthroplasty problems. Rapid manufacture of patient-specific implants via 3D printing can lessen the form effect.

3. MATERIAL AND METHODS

3.1 Material Selection

Because there are several dependent criteria involved, choosing the right material for orthopaedic implants—particularly hip implants—is a challenging integrated effort. Although hemiarthroplasty, also referred to as total arthroplasty, uses natural tissue, it is significantly impacted by the increase in wear over time. The selection criteria,

which provide more cost-effective and high-performing material, are based on a number of factors, including chemical, biological, physical, economic, and mechanical elements. The prior focus is the materials contact analysis, which provides a precise definition of the wear characteristics. Ceramic over polyethylene, metal over metal, ceramic over ceramic, and metal over polyethylene are the materials that are typically examined for contact analysis in relation to hip implants.

The prospect of a new era hemiarthroplasty as an alternative to a complete arthroplasty using new, contemporary materials and production procedures are investigated. The hemiarthroplasty preserves the native bone of the acetabulum while replacing the ball-shaped part of the femur. With this modification, a total hip replacement is typically preferred. When the ball component of the femoral bone is replaced in the hip joint, the socket portion of the hip bone remains intact. It is difficult to choose the best orthopaedic material in every way. It is difficult to design novel implant materials while adhering to production constraints. The process of choosing materials is influenced by a number of elements, but it often revolves around key characteristics, biocompatibility, and cost. When choosing implants, an orthopaedic surgeon typically takes the patient's age, degree of activity, and active/laidback lifestyle into account. Metal-on-polymer (MoP) implants have significant issues with material wear, which finally has an adverse effect on joint anatomy over time. When it comes to implants, metal-on-metal (MoM) implants show less wear than MoP implants. This implant has the least degree of wear, yet it releases extremely poisonous metallic ions. In contrast to stainless steel, cobalt-chromium alloys are often used materials to reduce the impact of metallic ions. Ceramic on polymer - Metallic ions can be reduced drastically with a ceramic femoral ball. Ceramic on ceramic- CoC has the lowest metallic ion release of among all prosthesis.

NbTiZrMo alloy on bone- Out of all the metals and alloys, this material is the newest biomaterial lot with a modulus that is closer to cortical bone. Peek on bone- In order to maximize the positive effects of hemiarthroplasty while minimizing the negative ones, we are currently attempting to articulate PEEK femoral bone on cartilage.

Table 1. Material properties [46]

Properties (Units)	**Nb35Ti25Zr5MoAlloy**	**PEEK**	**CFR PEEK**
Density (kg/mm3)	7.45E-06	1.23E-06	1.53E-06
Young's modulus (MPa)	8.96E+13	3760	4500
Poisson's ratio	0.4	0.3	0.3
Bulk modulus (MPa)	7.47E+13	3133.3	3750
Shear modulus (MPa)	3.45E+13	1446.2	1730.8

The NbTiZrMo alloy, PEEK, and CFR-PEEK are the materials taken into consideration for the hip implant in this investigation; Table 1 lists their characteristics. The goal of hemiarthroplasty is to prevent stress shielding by using implant material with low stiffness. Nb35Ti25Zr5Mo (Annealed) has an elastic modulus of 13 msi (13000 ksi) (89.63 GPa). Few materials meet the condition that the implant material be closer to the cortical bone for a better hemiarthroplasty, as we can analyze. With 90 GPa, Nb35Ti25Zr5Mo is ideal for enamel (GPa=40–83), meaning it is used in dentistry rather than orthopedics.

Most significantly, the titanium-niobium alloy is nontoxic and has outstanding mechanical strength and machinability. Stress-shielding issues and post-operative problems are caused by the high Young's modulus of Ti-based alloys. Better stress transfer along the bone, particularly around bone implants, is induced by a modulus. Ideally, this will bone safely. It can be a great option for an orthopaedic implant because of its greater corrosion resistance and flexibility closer to the bone. This alloy has an elastic modulus of about 90 GPa, which is rather low when you consider all bio-metals utilized in orthopaedic implants.

Because PEEK and titanium share similar mechanical properties, PEEK material shows less stress shielding than titanium. According to recent research, enhancing PEEK's bioactive qualities at the nanoscale will make it more suitable for use in human implants. It has also been noted that by taking into account the characteristics of the bone, materials with a lower Young's modulus can be used to increase the biocompatibility of the implants. The titanium alloys have a greater degree of stress shielding due to their higher Young's modulus. In the local tissue, this can occasionally fail. Because PEEK is more similar to bone characteristics and has lower Young's modulus values than titanium, it is a perfect choice for biomedical implants [46].

CFR-PEEK is a material that was taken from the aircraft industry, which has similar strict requirements. For the past three decades, Peek has been widely used in the dental, spine, and cranial fields because of its mechanical qualities and biocompatibility. Reinforced with carbon fibre. The type of PEEK that has been used extensively in spinal implants is CFR-PEEK, which has the tensile strength and Young's modulus closest to cortical bone. Regular PEEK is not appropriate for high load-bearing applications like the knee and hip because to its mechanical strength deficiencies.

The selection of NbTiZrMo alloy, PEEK, and CFR-PEEK was based on their distinct mechanical and biomechanical characteristics representing three major classes of implant materials: metallic, polymeric, and composite biomaterials. NbTiZrMo alloy was chosen due to its high strength and corrosion resistance, although its relatively high stiffness may contribute to stress shielding. PEEK was selected for its low elastic modulus and biocompatibility, enabling improved load transfer to the surrounding bone; however, its lower mechanical strength limits its suitability for high load-bearing applications. CFR-PEEK was included as an advanced composite material that offers a balanced combination of stiffness and strength, closely matching the mechanical properties

of cortical bone. This comparative selection enables a comprehensive evaluation of material behavior across a wide stiffness spectrum relevant to orthopedic implant design.

3.2 Method

The human anatomy consists of the femoral head, which is a smaller, convex sphere, implanted or engrafted in the acetabulum, which is a bigger, concave hemisphere or cup. In this instance, the relationship between hip motion and resulting load is described using three coordinate systems, as illustrated in Figure 3. On the right side of the femoral head, in the center, is an absolute coordinate system consisting of X, Y, and Z. The backside-prior is Yaxis, the median-sidelong is X-axis, and the facade plane is XZ in the absolute coordinate system.

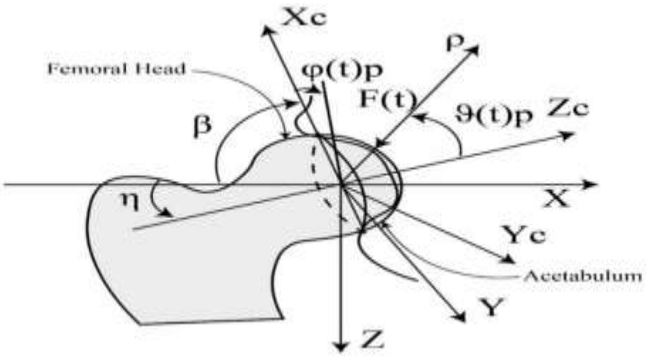

Figure 2. Coordinate system for the femur head in analytical analysis [46].

The second coordinate system is located at the centre of the cup Xc, Yc, and Zc. The Xc and Yc axes point toward the cup's front, and the cup flat face plane is Xc-Yc. The cup inclination angle is "β," the angle created by the axis X and Xc. The cup ante version angle is "η," the angle created by the axis X and Zc. The point "P," which is located on the articular surface, receives the resulting load vector F (t). On the articular surface axis Xc, Yc, and Zc, there is also a spherical coordinate system made up of ρ, θ, and φ. According to the anatomy, the femur head is hemispherical in shape and has a smooth surface with new state gristle. It reflects the surface with edge contact of the femoral head into the acetabulum and is based on the loading and stress distribution of the head with a cup. In this work, the stress distribution is taken into consideration using the Hertzian hypothesis, which is commonly applied when in contact with nonconforming geometrical objects[]. The complete calculations are in the next section.

3.3 Stress Shielding

Hip implants are supposed to last 20 years, however a multitude of problems reduce that time; the main reason for deterioration is stress shielding. By employing a femoral ball made of PEEK or coated with peek, which has properties closer to the bone, the aim is to lessen wear and strain cartilage.

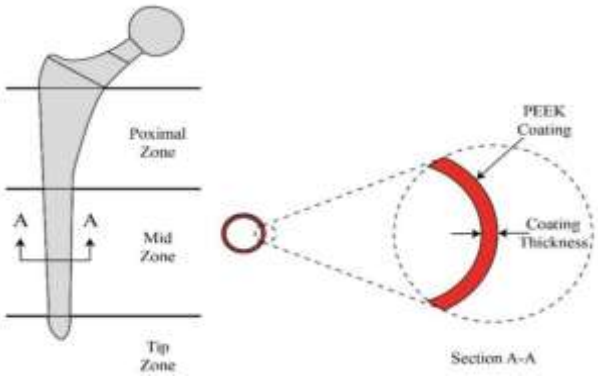

Figure 3. Different zones in hip implant steam and PEEK coating [46].

3.4 Modeling and Meshing

The properties of the three materials are briefly described in the section above before they are used for the finite element analysis. The simulations were performed using ANSYS Workbench 16.2 with static structural analysis. Tetrahedral elements were used for meshing, and contact interactions were defined as frictionless contact between implant and bone surfaces. The material behavior was assumed to be linear elastic and isotropic. Boundary conditions were applied by fixing the acetabular region, while loads ranging from 2200 N to 2800 N were applied along the femoral axis to simulate physiological conditions. Figure 4 (a) displays the implant's three-dimensional model. The following are the several steps that make up the finite element analysis process used in this study:

• Computed tomography (CT) is used to scan the actual femur bone, and the images are then imported into the for-profit SolidWorks program.

• SolidWorks, a 3D modelling program, is used to model the implant and create a three-dimensional model of the femur bone.

• After being transformed into STP file format, the implant model is imported into ANSYS Workbench 16.2 for examination.

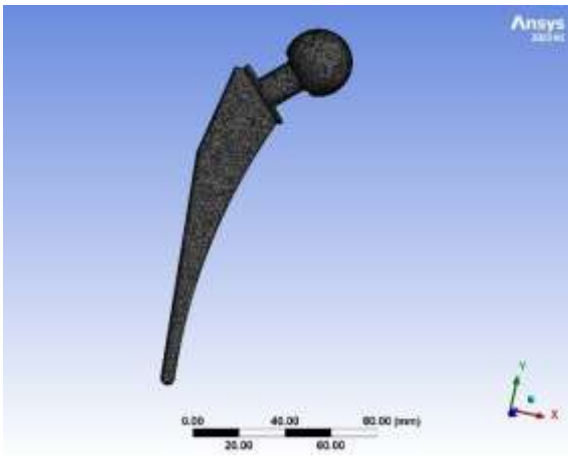

Figure 4 (a) The implant's three-dimensional model

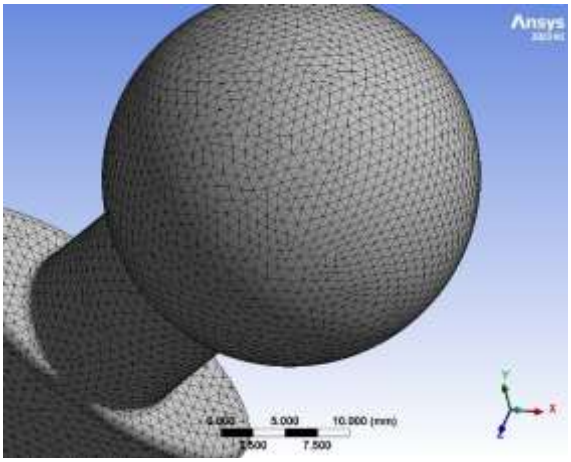

Figure 4(b) The meshed view

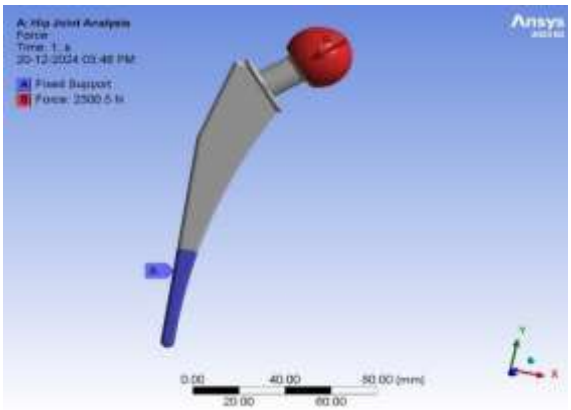

Figure 4(c) Loading and boundary conditions

Unstructured mesh techniques are used for meshing in this paper. An internal stem taper of 30 has been used to approximate the typical implant. In 3D analysis, the meshing type is regarded as tetrahedral. Due to the complex component shape, the grid's size is not set. The femoral head receives a transverse force of 2200–2500 N from the femoral neck. ASTM F2996-13 and ISO 7206-4:2010 are utilized (E) to establish the weights and boundary conditions. Figure 4(b) displays the meshed view, whereas Figure 4(c) displays the loading and boundary conditions.

3.5 Mesh Convergence Study

To ensure numerical accuracy and solution stability, a mesh convergence study was performed by progressively refining the element size and monitoring the variation in Von Mises stress. Tetrahedral elements were employed, and multiple mesh densities were analyzed. It was observed that beyond a mesh size of approximately 1.5 mm, the variation in stress values was less than 2%, indicating mesh independence of the solution. Therefore, this mesh configuration was adopted for all subsequent simulations to balance computational efficiency and accuracy.

Table 2. Mesh Convergence Study

Element Size (mm)	Number of Elements	Von-Mises Stress (MPa)
3.0	85,200	318.5
2.5	112,400	322.1
2.0	148,750	324.8
1.5	196,300	325.6
1.2	245,800	326.1

It can be observed that the variation in stress values becomes minimal beyond an element size of 1.5 mm, and therefore, this mesh size was selected for further simulations.

4. RESULT AND DISCUSSIONS

4.1 Validation

The three-dimensional model of the implant was built and validated in order to support the current study. The fixed support, which is applied at the apex of the acetabulum's lip, is one of the boundary conditions in this FEA procedure. 2200 N is the applied load. The bottom portion of the femur head, where the steam is attached, is subjected to the load. In this model, the load is applied in the Y direction, which is perpendicular. The femur head is subjected to displacement in order to limit its range of motion. The femur head's range of motion is freely restricted in the Y direction. Figure 5 displays the boundary conditions used in this investigation.

The results obtained through the FEA for the implant comprise the equivalent elastic strain, contact pressure and equivalent Von Mises stress is validated with available literature [46] and found the good agreement with them as shown in Table 3.

Table 3. Validation of FEA results of selected materials between [44] and Present FEA results

Material	a^*	$a^\#$	b^*	$b^\#$	c^*	$c^\#$
NbTiZrMo Alloy	8.34e-4	7.98e-4	1.3988	1.2678	8.5187	8.4479
PEEK	7.45e-4	7.27e-4	5.0351	4.9785	8.1028	8.0845
CFR-PEEK	7.56e-4	7.46e-4	1.5006	1.4796	8.446	8.4015

[44]= Pimpale et al., (2022), # =Present Work; a= Equivalent Elastic Strain, b= Contact pressure (MPa) and c= Von-Mises stress at bone (MPa)

The obtained results were validated by comparing the equivalent stress, strain, and contact pressure values with previously published studies [46]. The deviation between the present results and literature values was found to be within 5%, indicating good agreement (As shown in Table 3) and confirming the reliability of the numerical model. The developed finite element model was validated by comparing the obtained results with previously published numerical and experimental studies. Key parameters including equivalent elastic strain, contact pressure, and Von Mises stress showed good agreement with literature values, with deviations within 5%. This level of agreement confirms the reliability and accuracy of the present numerical model for evaluating hip implant biomechanics.

4.2 Effect of Material on Implant

Following validation, the current proposed customized implant was made using the three different materials. A load of between 2200 and 2500 N was applied throughout the analysis. The force type is constant magnitude ramped force, and the section discusses both the direction and the magnitude. Displacement constraints are used to limit the femur head's vertical motion in order to simplify and shorten the computation time. Only a hip contact force is used at one stage in the loading process, whereas additional reduced muscle loading was used in conjunction with the hip contact force to load the construct and undamaged bone. At the nodes of an element that are situated at contact points, the force is applied vertically. The realistic loads used to test hip implants for the maximum loads of 2500N body weight were the source of the load taken into consideration for optimization.

This section describes the findings of the finite element analysis (FEA) for the models of arthroplasty and hemiarthroplasty under varied load scenarios and material types. Equivalent Elastic Strain, Von-Mises Stress, Contact Pressure, and Total Deformation were all included in the analysis.

4.3 Arthroplasty Model

The performance of NbTiZrMo Alloy, PEEK, and CFR-PEEK under increasing loads of 2200, 2500, and 2800 N is displayed in Tables 3–5 for the Arthroplasty model. Because strain and stress are directly proportional in linear elastic circumstances, the equivalent elastic strain for all materials rose as the applied load increased. The NbTiZrMo alloy's strong stiffness, which lessens deformation, allowed it to show the lowest strain values under all loads. But because of this property, the material is more likely to experience stress shielding, which can erode the surrounding bone. PEEK, on the other hand, showed the highest strain values, suggesting that it was more flexible and less stiff; however, this extreme deformation would make it less able to support long-term pressures. There was moderate strain in CFR-PEEK., balancing flexibility and stiffness, making it more suitable for reducing stress shielding while maintaining structural stability.

For all materials, the Von-Mises Stress on the implant rose as the load increased. Because of its inefficient load distribution, which concentrates stress in certain areas, NbTiZrMo Alloy continuously displayed the highest stress values. Although PEEK had the lowest Von-Mises Stress, its significant deformation prevents it from being used

in real-world situations. Intermediate stress values were demonstrated by CFR-PEEK, which efficiently distributed the load while preserving the implant's structural integrity.

Table 4. Result of equivalent elastic strain for both bone and model (Arthroplasty)

Load (10^3 N)	Material	Equivalent Elastic Strain (Bone)	Equivalent Elastic Strain (Model)
2.2	NbTiZrMo Alloy	0.0023	0.0018
2.5	NbTiZrMo Alloy	0.0027	0.0022
2.8	NbTiZrMo Alloy	0.0031	0.0025
2.2	PEEK	0.003	0.0024
2.5	PEEK	0.0035	0.0028
2.8	PEEK	0.004	0.0031
2.2	CFR-PEEK	0.0028	0.0021
2.5	CFR-PEEK	0.0032	0.0025
2.8	CFR-PEEK	0.0036	0.0028

Table 5. Result of contact pressure (Arthroplasty)

Load (10^3 N)	Material	Contact Pressure (MPa)
2.2	NbTiZrMo Alloy	15.2
2.5	NbTiZrMo Alloy	17.8
2.8	NbTiZrMo Alloy	20.1
2.2	PEEK	12.7
2.5	PEEK	14.9
2.8	PEEK	17.3
2.2	CFR-PEEK	14.3
2.5	CFR-PEEK	16.6
2.8	CFR-PEEK	19.1

Table 6. Result of equivalent elastic strain for both bone and model (Arthroplasty)

Load (10^3 N)	Material	Von-Mises Stress (Bone, MPa)	Von-Mises Stress (Model, MPa)
2.2	NbTiZrMo Alloy	85.6	320.3
2.5	NbTiZrMo Alloy	95.1	368.2
2.8	NbTiZrMo Alloy	102.7	402.5
2.2	PEEK	78.4	195.1
2.5	PEEK	86.3	220.5
2.8	PEEK	94	243.6
2.2	CFR-PEEK	82	252.4
2.5	CFR-PEEK	89.7	285.7
2.8	CFR-PEEK	97.2	312.6

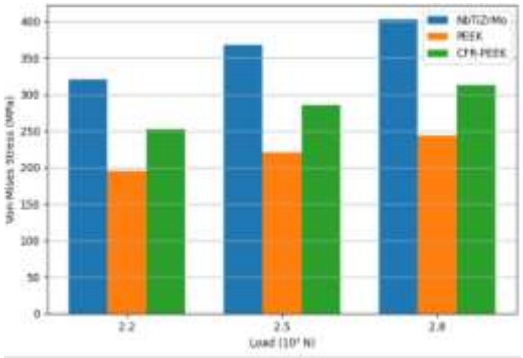

Figure 5 Comparison of Von-Mises stress for different implant materials under varying loads for arthroplasty condition

The Figure 5 shows that the Von-Mises stress in the implant model increases continuously with increase in load from 2.2 × 10^3 N to 2.8 × 10^3 N for all three materials. Among the selected materials, NbTiZrMo alloy exhibits the highest stress values at all loading conditions, indicating its higher stiffness and greater stress concentration in the implant model. PEEK shows the lowest stress values, whereas CFR-PEEK gives intermediate stress values. This trend indicates that CFR-PEEK provides a more balanced mechanical response than NbTiZrMo alloy while maintaining better structural performance than PEEK under arthroplasty condition.

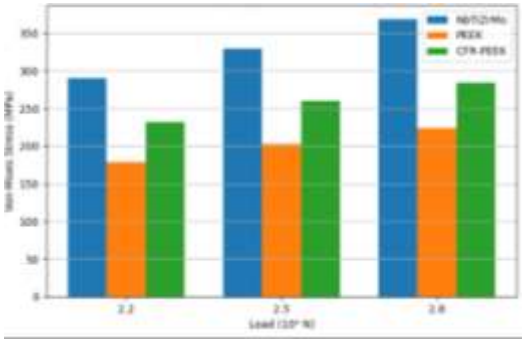

Figure 6 Comparison of Von-Mises stress for different implant materials under varying loads for hemiarthroplasty condition

The Figure 6 also indicates a steady increase in Von-Mises stress with increasing load for all materials. Similar to the arthroplasty case, NbTiZrMo alloy produces the highest stress values, PEEK shows the lowest stress values, and CFR-PEEK lies in between. However, the overall stress values in hemiarthroplasty are lower than those observed in arthroplasty for the same material and loading condition. This suggests that hemiarthroplasty offers comparatively better stress distribution, likely due to the contribution of the natural acetabular surface in sharing the applied load.

For all materials, contact pressure—a measurement of the force applied at the bone-implant interface—also rose as the load increased. The highest contact pressure was recorded by PEEK, which may cause the bone and cartilage to deteriorate more quickly. CFR-PEEK, on the other hand, reduced the chance of tissue damage by maintaining moderate contact pressure levels. Despite having a low contact pressure, NbTiZrMo Alloy is constrained by its propensity to induce stress shielding.

The implant's total deformation increased with load in a similar manner. PEEK further shown its unsuitability for load-bearing applications by exhibiting the maximum distortion under all loads. Better durability and resistance to failure under repeated loading were ensured by CFR-PEEK's much reduced deformation when compared to PEEK. NbTiZrMo Alloy exhibited minimal deformation, consistent with its high stiffness, but its negative implications on bone health remain a concern.

4.4 Hemiarthroplasty Model

The performance of the three materials under Hemiarthroplasty conditions is summarized in Table 7 – Table 8. Similar trends were observed for Equivalent Elastic Strain, Von-Mises Stress, Contact Pressure, and Total Deformation.

Table 7. Result of equivalent elastic strain for both bone and model (Hemiarthroplasty)

Load (10^3 N)	Material	Equivalent Elastic Strain (Bone)	Equivalent Elastic Strain (Model)
2.2	NbTiZrMo Alloy	0.0019	0.0015
2.5	NbTiZrMo Alloy	0.0023	0.0019
2.8	NbTiZrMo Alloy	0.0027	0.0022
2.2	PEEK	0.0026	0.002
2.5	PEEK	0.003	0.0024
2.8	PEEK	0.0035	0.0027
2.2	CFR-PEEK	0.0024	0.0018
2.5	CFR-PEEK	0.0028	0.0021
2.8	CFR-PEEK	0.0032	0.0024

Table 8. Result of contact pressure (Hemiarthroplasty)

Load (10^3 N)	Material	Contact Pressure (MPa)
2.2	NbTiZrMo Alloy	14.1
2.5	NbTiZrMo Alloy	16.5
2.8	NbTiZrMo Alloy	18.8
2.2	PEEK	11.9
2.5	PEEK	14.1
2.8	PEEK	16.4
2.2	CFR-PEEK	13.3
2.5	CFR-PEEK	15.6
2.8	CFR-PEEK	18

Table 9. Result of Von-mises stress for both bone and model (Hemiarthroplasty)

Load (10^3 N)	Material	Von-Mises Stress (Bone, MPa)	Von-Mises Stress (Model, MPa)

2.2	NbTiZrMo Alloy	78.3	290.4
2.5	NbTiZrMo Alloy	86.2	329.5
2.8	NbTiZrMo Alloy	93.7	368.3
2.2	PEEK	72.6	178.7
2.5	PEEK	79.5	202.5
2.8	PEEK	87	223.9
2.2	CFR-PEEK	75.4	232.1
2.5	CFR-PEEK	82	260.3
2.8	CFR-PEEK	89.3	284.6

For all materials, the results for Equivalent Elastic Strain rose as the applied load increased. Despite its high stiffness and increased danger of stress shielding, NbTiZrMo alloy showed the least strain. Although PEEK is flexible, it is not appropriate for high-load situations, as seen by the maximum strain values it displayed. With modest strain values that reduce stress shielding and permit sufficient flexibility for natural load transfer, CFR-PEEK offered the best possible balance.

The Von-Mises Stress also increased with the load. The highest stress values were observed by NbTiZrMo Alloy, indicating its ineffective stress dissipation. Although PEEK had the lowest stress levels, its significant deformation once more placed restrictions on it. By striking a balance between stress dissipation and structural stability, CFR-PEEK showed moderate stress levels.

Contact As the load increased, so did the pressure at the bone-implant interface. The greatest levels were obtained by PEEK, which may cause harm to natural tissue and cartilage. Comparatively, CFR-PEEK ensured less tissue damage by maintaining a moderate contact pressure. Despite having the lowest contact pressure, NbTiZrMo Alloy's stiffness-induced stress shielding makes long-term performance difficult.

PEEK was unsuitable for load-bearing implants because it displayed the greatest values of total deformation, which followed a similar pattern. CFR-PEEK showed little deformation, guaranteeing the implant's stability and lifespan. NbTiZrMo Alloy's mechanical rigidity was consistent with its minimal deformation, but it still has the potential to cause long-term problems.

Graphical comparisons of stress, strain, and contact pressure variations with respect to load and material type were generated to enhance visualization. These plots clearly indicate that CFR-PEEK maintains a balanced mechanical response compared to other materials.

A direct comparison between arthroplasty and hemiarthroplasty models reveals that hemiarthroplasty exhibits relatively lower stress concentrations and contact pressure due to the presence of natural acetabular cartilage. On average, stress values in hemiarthroplasty models were found to be 8–12% lower than those in arthroplasty models under similar loading conditions.

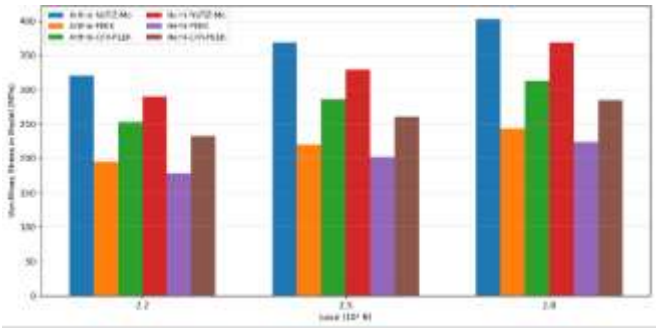

Figure 7. Combined comparison of Von-Mises stress in the implant model for arthroplasty and hemiarthroplasty conditions at different loading levels.

The combined graph clearly demonstrates the comparative biomechanical behavior of arthroplasty and hemiarthroplasty models under identical loading conditions. For every material and at each load level, the hemiarthroplasty model exhibits lower Von-Mises stress than the corresponding arthroplasty model. In both implant configurations, NbTiZrMo alloy produces the maximum stress, PEEK gives the minimum stress, and CFR-PEEK shows moderate stress values. This combined comparison confirms that hemiarthroplasty has a relative advantage in reducing implant stress, while CFR-PEEK remains the most balanced material due to its favorable combination of strength and flexibility.

A direct comparative assessment indicates that hemiarthroplasty configurations yield approximately 8–12% lower stress levels and reduced contact pressure compared to arthroplasty under identical loading conditions, highlighting their improved load-sharing capability and biomechanical efficiency.

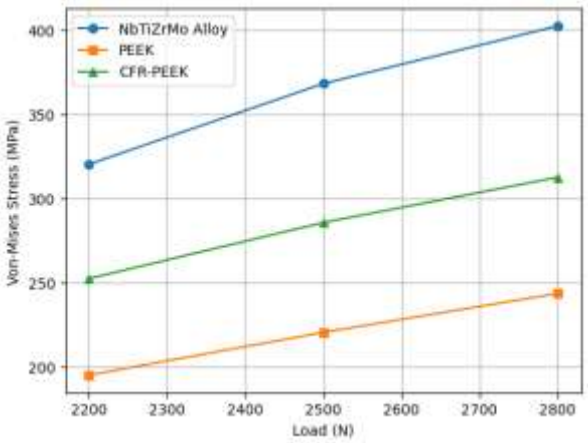

(A) Load vs Von-Mises Stress (for all 3 materials)

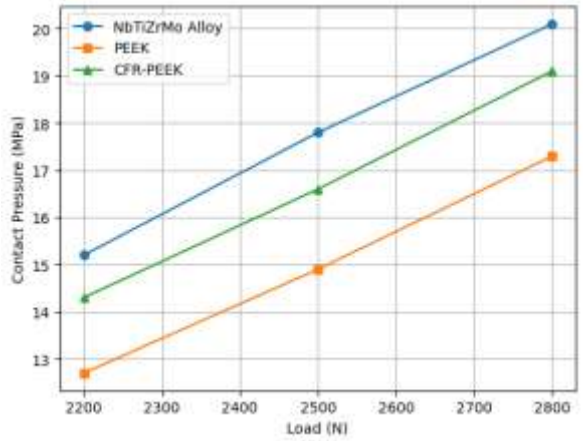

(B) Load vs Contact Pressure

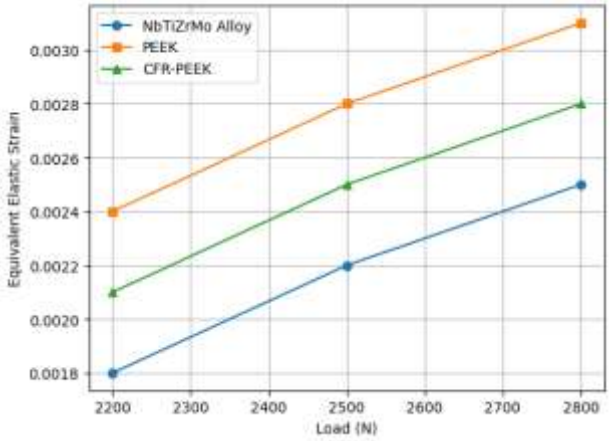

(C) Load vs Equivalent Strain

Figure 8. Comparison of Von-Mises stress for NbTiZrMo alloy, PEEK, and CFR-PEEK under varying physiological loads.

A graphical comparison of the biomechanical parameters reveals a consistent trend across all loading conditions, where NbTiZrMo alloy exhibits the highest stress values, while PEEK shows the lowest stress but excessive deformation. CFR-PEEK demonstrates intermediate stress levels with significantly improved load distribution characteristics. The plotted results clearly indicate that CFR-PEEK achieves a balanced mechanical response by minimizing stress concentration while avoiding excessive deformation, making it more suitable for load-bearing orthopedic applications.

4.5 Comparative Analysis

A direct comparison between arthroplasty and hemiarthroplasty models under identical loading conditions reveals that hemiarthroplasty consistently exhibits lower stress concentrations and contact pressures. Quantitatively, the Von-Mises stress in hemiarthroplasty models is approximately 8–12% lower than that observed in arthroplasty across all materials. This reduction is attributed to the presence of the natural acetabular surface, which facilitates improved load sharing and reduces localized stress accumulation. These findings indicate that implant

configuration plays a significant role in biomechanical performance and should be considered alongside material selection.

From a clinical perspective, reducing stress shielding and maintaining physiological load transfer are essential for preventing bone resorption and ensuring long-term implant stability. Materials with high stiffness, such as NbTiZrMo alloy, may lead to stress shielding and subsequent implant loosening, whereas excessively flexible materials like PEEK may result in structural instability under high loads. CFR-PEEK offers a favorable balance by closely matching the mechanical properties of cortical bone, thereby promoting uniform stress distribution and minimizing the risk of implant failure. Additionally, the lower stress levels observed in hemiarthroplasty suggest potential advantages in preserving bone integrity and reducing revision rates in suitable patient populations.

5. CONCLUSION

This study presents a comprehensive finite element evaluation of hip implant biomechanics by comparing arthroplasty and hemiarthroplasty configurations using three biomaterials: NbTiZrMo alloy, PEEK, and CFR-PEEK under physiological loading conditions (2200–2800 N). The results demonstrate clear material-dependent variations in biomechanical performance. Quantitatively, CFR-PEEK exhibits a reduction in Von-Mises stress of approximately 18–25% compared to NbTiZrMo alloy, while maintaining significantly lower deformation than PEEK, which shows the highest strain values (up to ~0.0031 under 2800 N). In contrast, NbTiZrMo alloy, although mechanically stiff, produces the highest stress concentrations (up to ~402 MPa), indicating a higher risk of stress shielding.

A direct comparison between implant configurations reveals that hemiarthroplasty consistently produces 8–12% lower stress levels and reduced contact pressure compared to arthroplasty under identical loading conditions. This improvement is attributed to the presence of the natural acetabular surface, which enhances load-sharing and reduces localized stress concentration. These findings confirm that both material selection and implant configuration play a critical role in determining overall biomechanical performance.

The numerical results show good agreement with previously reported studies, with deviations within approximately 5%, thereby validating the reliability of the developed finite element model. From a clinical standpoint, minimizing stress shielding while maintaining adequate structural stability is essential for preventing bone resorption and improving implant longevity. In this context, CFR-PEEK demonstrates a favorable balance between stiffness and flexibility, closely matching the mechanical behavior of cortical bone.

The key contribution of this study lies in the integrated evaluation of stem taper geometry, advanced biomaterials, and implant configuration within a unified finite element framework, which has not been sufficiently addressed in prior research. Unlike earlier studies that considered these parameters independently, the present work establishes a direct relationship between taper design, material properties, and implant stability.

Based on the findings, CFR-PEEK is recommended as a superior material for hip implant applications, particularly in cases where reduction of stress shielding and improved load transfer are critical. Additionally, hemiarthroplasty may be preferred in selected clinical scenarios where preservation of the natural acetabulum is feasible, due to its lower stress characteristics. Future work should focus on dynamic loading conditions, fatigue analysis, and experimental or clinical validation to further substantiate these findings and support their translation into surgical practice.

Declaration of Interests

The authors declare that they have no known competing financial interests or personal relationships that could have appeared to influence the work reported in this paper.

Funding Information

Authors state no funding involved.

Author Contribution

The authors confirm contribution to the paper as follows: Study Conception and Design: Siddharth Tiwari and N.K. Jain; Data Collection: Siddharth Tiwari; Analysis and Interpretation of Results: Siddharth Tiwari and N.K. Jain; Draft Manuscript Preparation: Siddharth Tiwari and N.K. Jain. All authors reviewed the results and approved the final version of the manuscript.

Data Availability Statement

The data that support the findings of this study are available from the author upon reasonable request.

Research Involving Human And /Or Animals

Not applicable

Informed Consent

Not applicable

REFERENCES

1. Garofalo, S., Morano, C., Bruno, L., & Pagnotta, L.,“A comprehensive literature review for total hip arthroplasty (THA): Part 2—Material selection criteria and methods,” *Journal of Functional Biomaterials,* Vol. 16, no. 5, pp. 184, 2025. https://doi.org/10.3390/jfb16050184

2. Kalayarasan, M., & Shankar, S., "Mechanical loading characteristics of total hip prosthetics subjected to dynamic loading cycles," *Bio-Medical Materials and Engineering*, vol. 29, no. 6, pp. 663–676, 2018. https://doi.org/10.3233/BME-181019
3. G. Bergmann *et al.*, "Hip contact forces and gait patterns from routine activities," *Journal of Biomechanics*, vol. 34, no. 7, pp. 859–871, Jul. 2001, doi: https://doi.org/10.1016/s0021-9290(01)00040-9.
4. D. E. Lunn, A. Lampropoulos, and T. D. Stewart, "Basic biomechanics of the hip," *Orthopaedics and Trauma*, vol. 30, no. 3, pp. 239–246, Jun. 2016, doi: https://doi.org/10.1016/j.mporth.2016.04.014.
5. L. Gao, P. Yang, I. Dymond, J. Fisher, and Z. Jin, "Effect of surface texturing on the elastohydrodynamic lubrication analysis of metal-on-metal hip implants," *Tribology International*, vol. 43, no. 10, pp. 1851–1860, Oct. 2010, doi: https://doi.org/10.1016/j.triboint.2010.02.006
6. Azim Ataollahi Oshkour, Noor, M. Bayat, R. Afshar, and F. Berto, "Three-dimensional finite element analyses of functionally graded femoral prostheses with different geometrical configurations," *Materials in engineering*, vol. 56, pp. 998–1008, Apr. 2014, doi: https://doi.org/10.1016/j.matdes.2013.12.054.
7. J. J. Williams and N. Chawla, "Fractography of a neck failure in a double-modular hip implant," *Case Studies in Engineering Failure Analysis*, vol. 2, no. 1, pp. 45–50, Apr. 2014, doi: https://doi.org/10.1016/j.csefa.2014.03.001.
8. T. A. Maxian, T. D. Brown, D. R. Pedersen, and J. J. Callaghan, "A sliding-distance-coupled finite element formulation for polyethylene wear in total hip arthroplasty," *Journal of Biomechanics*, vol. 29, no. 5, pp. 687–692, May 1996, doi: https://doi.org/10.1016/0021-9290(95)00125-5.
9. B. R. Burroughs, B. Hallstrom, G. J. Golladay, D. Hoeffel, and W. H. Harris, "Range of Motion and Stability in Total Hip Arthroplasty With 28-, 32-, 38-, and 44-mm Femoral Head Sizes," *The Journal of Arthroplasty*, vol. 20, no. 1, pp. 11–19, Jan. 2005, doi: https://doi.org/10.1016/j.arth.2004.07.008.
10. J.-M.S. Lamvohee, R. Mootanah, P. Ingle, K. Cheah, and J. K. Dowell, "Stresses in cement mantles of hip replacements: effect of femoral implant sizes, body mass index and bone quality," *Computer Methods in Biomechanics & Biomedical Engineering*, vol. 12, no. 5, pp. 501–510, Feb. 2009, doi: https://doi.org/10.1080/10255840902718626.
11. K. Chalernpon, P. Aroonjarattham, and K. Aroonjarattham, "Static and Dynamic Load on Hip Contact of Hip Prosthesis and Thai Femoral Bones," *World Academy of Science, Engineering and Technology, International Journal of Mechanical and Mechatronics Engineering*, vol. 2, no. 3, pp. 251–255, Mar. 2015.
12. S. Hussenbocus, D. Kosuge, L. B. Solomon, D. W. Howie, and R. H. Oskouei, "Head-Neck Taper Corrosion in Hip Arthroplasty," *BioMed Research International*, vol. 2015, 2015, doi: https://doi.org/10.1155/2015/758123.
13. A. C. Cilingir, "Finite element analysis of the contact mechanics of ceramic-on-ceramic hip resurfacing prostheses," *Journal of Bionic Engineering*, vol. 7, no. 3, pp. 244–253, Sep. 2010, doi: https://doi.org/10.1016/s1672-6529(10)60247-8.
14. Daniel Panghihutan Malau *et al.*, "Finite element analysis of porous stemmed hip prosthesis for children," *AIP Conference Proceedings*, Jan. 2019, doi: https://doi.org/10.1063/1.5139393.
15. T. Çelik and Y. Kişioğlu, "Evaluation of new hip prosthesis design with finite element analysis," *Australasian Physical & Engineering Sciences in Medicine*, vol. 42, no. 4, pp. 1033–1038, Oct. 2019, doi: https://doi.org/10.1007/s13246-019-00802-0.
16. D. Royhman *et al.*, "Fretting-corrosion in Hip Implant Modular Junctions: New Experimental Set-up and Initial Outcome," *Tribology international*, vol. 91, pp. 235–245, Nov. 2015, doi: https://doi.org/10.1016/j.triboint.2015.04.032.
17. G. A. Turley, D. R. Griffin, and M. A. Williams, "Effect of femoral neck modularity upon the prosthetic range of motion in total hip arthroplasty," *Medical & Biological Engineering & Computing*, vol. 52, no. 8, pp. 685–694, Jun. 2014, doi: https://doi.org/10.1007/s11517-014-1171-9.
18. R. Bader, R. Scholz, E. Steinhauser, S. Zimmermann, R. Busch, and W. Mittelmeier, "The influence of head and neck geometry on stability of total hip replacement," *Acta Orthopaedica*, vol. 75, no. 4, pp. 1–1, Aug. 2004, doi: https://doi.org/10.1080/759369184.
19. G. B. Higgs *et al.*, "Does Taper Size Have an Effect on Taper Damage in Retrieved Metal-on-Polyethylene Total Hip Devices?," *The Journal of Arthroplasty*, vol. 31, no. 9, pp. 277–281, Sep. 2016, doi: https://doi.org/10.1016/j.arth.2016.06.053.
20. T. Bitter, I. Khan, T. Marriott, E. Lovelady, N. Verdonschot, and D. Janssen, "The effects of manufacturing tolerances and assembly force on the volumetric wear at the taper junction in modular total hip arthroplasty," *Computer Methods in Biomechanics and Biomedical Engineering*, vol. 22, no. 13, pp. 1061–1072, Jun. 2019, doi: https://doi.org/10.1080/10255842.2019.1627524.
21. K. C. N. Kumar, T. Tandon, P. Silori, and A. Shaikh, "Biomechanical Stress Analysis of a Human Femur Bone Using ANSYS," *Materials Today: Proceedings*, vol. 2, no. 4–5, pp. 2115–2120, 2015, doi: https://doi.org/10.1016/j.matpr.2015.07.211.
22. T. S. Antonio, M. Ciaccia, C. Müller-Karger, and E. Casanova, "Orientation of orthotropic material properties in a femur FE model: A method based on the principal stresses directions," *Medical Engineering & Physics*, vol. 34, no. 7, pp. 914–919, Nov. 2011, doi: https://doi.org/10.1016/j.medengphy.2011.10.008.
23. S. Jade, K. H. Tamvada, D. S. Strait, and I. R. Grosse, "Finite element analysis of a femur to deconstruct the paradox of bone curvature," *Journal of Theoretical Biology*, vol. 341, pp. 53–63, Jan. 2014, doi: https://doi.org/10.1016/j.jtbi.2013.09.012.

24. A. E. Yousif, “Biomechanical Analysis of the human femur bone during normal walking and standing up,” *IOSR Journal of Engineering*, vol. 02, no. 08, pp. 13–19, Aug. 2012, doi: https://doi.org/10.9790/3021-02851319.
25. M. N. Rahaman, T. Huang, A. Yao, B. S. Bal, and Y. Li, “SiC nanoparticle-reinforced Al2O3–Nb composite as a potential femoral head material in total hip arthroplasty,” *Materials Science and Engineering: C*, vol. 30, no. 8, pp. 1197–1203, Oct. 2010,doi:https://doi.org/10.1016/j.msec.2010.06.012.
26. Ashkenazi, I., Benady, A., Ben Zaken, S., & Factor, S.,”Radiological comparison of canal fill between collared and non-collared femoral stems: A two-year follow-up after total hip arthroplasty,” Journal of Imaging, vol. 10, no. 5, pp. 99, 2024. https://doi.org/10.3390/jimaging10050099.
27. Y. Abu-Amer, I. Darwech, and J. C. Clohisy, “Aseptic loosening of total joint replacements: mechanisms underlying osteolysis and potential therapies,” Arthritis Research & Therapy, vol. 9, no. Suppl 1, p. S6, 2007, doi: https://doi.org/10.1186/ar2170.
28. C. Brockett, S. Williams, Z. Jin, G. Isaac, and J. Fisher, “Friction of total hip replacements with different bearings and loading conditions,” *Journal of Biomedical Materials Research Part B: Applied Biomaterials*, vol. 81B, no. 2, pp. 508–515, 2007, doi: https://doi.org/10.1002/jbm.b.30691.
29. V. Krenn *et al.*, “Revised histopathological consensus classification of joint implant related pathology,” *Pathology - Research and Practice*, vol. 210, no. 12, pp. 779–786, Dec. 2014, doi: https://doi.org/10.1016/j.prp.2014.09.017
30. C. Zietz, P. Bergschmidt, R. Lange, W. Mittelmeier, and R. Bader, “Third-Body Abrasive Wear of Tibial Polyethylene Inserts Combined with Metallic and Ceramic Femoral Components in a Knee Simulator Study,” The International Journal of Artificial Organs, vol. 36, no. 1, pp. 47–55, Jan. 2013, doi: https://doi.org/10.5301/ijao.5000189.
31. R. Bader, R. Scholz, E. Steinhauser, S. Zimmermann, R. Busch, and W. Mittelmeier, “The influence of head and neck geometry on stability of total hip replacement,” Acta Orthopaedica, vol. 75, no. 4, pp. 1–1, Aug. 2004, doi: https://doi.org/10.1080/759369184.
32. T Sorimachi, I. C. Clarke, P. A. Williams, A. Gustafson, and K. Yamamoto, “Third-body abrasive wear challenge of 32 mm conventional and 44 mm highly crosslinked polyethylene liners in a hip simulator model,” Proceedings of the Institution of Mechanical Engineers Part H Journal of Engineering in Medicine, vol. 223, no. 5, pp. 607–623, Apr. 2009, doi: https://doi.org/10.1243/09544119jeim562.
33. J. D. DesJardins, S. A. Banks, L. C. Benson, T. Pace, and M. LaBerge, “A direct comparison of patient and force-controlled simulator total knee replacement kinematics,” Journal of Biomechanics, vol. 40, no. 15, pp. 3458–3466, 2007, doi: https://doi.org/10.1016/j.jbiomech.2007.05.022.
34. D. Sarkar, S. Mandal, B. S. B. Reddy, N. Bhaskar, D.C. Sundaresh, and B. Basu, “ZrO2-toughened Al2O3-based near-net shaped femoral head: Unique fabrication approach, 3D microstructure, burst strength and muscle cell response,” *Materials Science and Engineering: C*, vol. 77, pp. 1216–1227, Aug. 2017, doi: https://doi.org/10.1016/j.msec.2017.03.123
35. V. Pakhaliuk, A. Polyakov, M. Kalinin, and V. Kramar, “Improving the Finite Element Simulation of Wear of Total Hip Prosthesis’ Spherical Joint with the Polymeric Component,” *Procedia Engineering*, vol. 100, pp. 539–548, 2015, doi: https://doi.org/10.1016/j.proeng.2015.01.401
36. D. Sarkar, B. S. B. Reddy, S. Mandal, M.V.S. Ravisankar, and B. Basu, “Uniaxial Compaction-Based Manufacturing Strategy and 3D Microstructural Evaluation of Near-Net-Shaped ZrO2-Toughened Al2O3Acetabular Socket,” Advanced Engineering Materials, vol. 18, no. 9, pp. 1634–1644, Jun. 2016, doi: https://doi.org/10.1002/adem.201600147.
37. R. Lee, A. Essner, A. Wang, and W. L. Jaffe, “Scratch and wear performance of prosthetic femoral head components against crosslinked UHMWPE sockets,” Wear, vol. 267, no. 11, pp. 1915–1921, Oct. 2009, doi: https://doi.org/10.1016/j.wear.2009.03.034.
38. W. L. Walter, G. C. O’Toole, W. K. Walter, A. Ellis, and B. A. Zicat, “Squeaking in Ceramic-on-Ceramic Hips,” The Journal of Arthroplasty, vol. 22, no. 4, pp. 496–503, Jun. 2007, doi: https://doi.org/10.1016/j.arth.2006.06.018.
39. J. C. Keurentjes, R. M. Kuipers, D. J. Wever, and B. W. Schreurs, “High Incidence of Squeaking in THAs with Alumina Ceramic-on-ceramic Bearings,” Clinical Orthopaedics & Related Research, vol. 466, no. 6, pp. 1438–1443, Jun. 2008, doi: https://doi.org/10.1007/s11999-008-0177-8.
40. G. B. Higgs et al., “Does Taper Size Have an Effect on Taper Damage in Retrieved Metal-on-Polyethylene Total Hip Devices?,” The Journal of Arthroplasty, vol. 31, no. 9, pp. 277–281, Sep. 2016, doi: https://doi.org/10.1016/j.arth.2016.06.053.
41. N. I. Galanis and D. E. Manolakos, “Surface roughness prediction in turning of femoral head,” The International Journal of Advanced Manufacturing Technology, vol. 51, no. 1–4, pp. 79–86, Apr. 2010, doi: https://doi.org/10.1007/s00170-010-2616-4.
42. C. Affolter, B. Weisse, A. Stutz, S Köbel, and G. P. Terrasi, “Optimization of the stress distribution in ceramic femoral heads by means of finite element methods,” Proceedings of the Institution of Mechanical Engineers Part H Journal of Engineering in Medicine, vol. 223, no. 2, pp. 237–248, Dec. 2008, doi: https://doi.org/10.1243/09544119jeim429.
43. G. Thrivikraman, P. K. Mallik, and B. Basu, “Substrate conductivity dependent modulation of cell proliferation and differentiation in vitro,” Biomaterials, vol. 34, no. 29, pp. 7073–7085, Sep. 2013, doi: https://doi.org/10.1016/j.biomaterials.2013.05.076.

44. L. Savarino et al., “Ion release in patients with metal-on-metal hip bearings in total joint replacement: A comparison with metal-on-polyethylene bearings,” vol. 63, no. 5, pp. 467–474, Jan. 2002, doi: https://doi.org/10.1002/jbm.10299.
45. J. H. Dumbleton, J. A. D’Antonio, M. T. Manley, W. N. Capello, and A. Wang, “The Basis for a Second-generation Highly Cross-linked UHMWPE,” Clinical Orthopaedics & Related Research, vol. 453, pp. 265–271, Dec. 2006, doi: https://doi.org/10.1097/01.blo.0000238856.61862.7d
46. “Experimental Investigation on Hip Implant Materials Development through Analytical and Finite Element Analysis: 3D Modelled Computed Tomography,” *Biointerface Research in Applied Chemistry*, vol. 12, no. 3, pp. 4103–4125, Aug. 2021, doi: https://doi.org/10.33263/briac123.41034125.